Magnetic and structural properties of the iron oxychalcogenides $La_2O_2Fe_2OM_2$ (M = S, Se)

B. Freelon,[1,*] Z. Yamani,[2] Ian Swainson,[3] R. Flacau,[2] B. Karki,[1] Yu Hao Liu,[4] L. Craco,[5] M. S. Laad,[6] Meng Wang,[7] Jiaqi Chen,[8] R. J. Birgeneau,[9,10,11] and Minghu Fang[8]

[1]*Department of Physics, University of Louisville, Louisville, Kentucky 40208, USA*
[2]*Canadian Nuclear Laboratories, Chalk River Laboratories, Chalk River, Ontario, Canada K0J 1J0*
[3]*Physics Section, International Atomic Energy Agency, Vienna International Centre, P.O. Box 100, 1400 Vienna, Austria*
[4]*Department of Materials Science and Engineering, University of Illinois Urbana Champaign, Urbana, Illinois 61801, USA*
[5]*Instituto de Fisica, Universidade Federal de Mato Grosso, 78060-900 Cuiaba, MT, Brazil*
[6]*The Institute of Mathematical Sciences, C.I.T. Campus, Chennai 600 113, India*
[7]*School of Physics, Sun Yat-Sen University, Guangzhou 510275, People's Republic of China*
[8]*Department of Physics, Zhejiang University, Hangzhou 310027, People's Republic of China*
[9]*Department of Physics, University of California, Berkeley, California 94720, USA*
[10]*Materials Science Division, Lawrence Berkeley National Laboratory, Berkeley, California 94720, USA*
[11]*Department of Materials Science and Engineering, University of California, Berkeley, California 94720, USA*

(Received 31 December 2017; revised manuscript received 28 December 2018; published 24 January 2019)

We present the results of structural and magnetic phase comparisons of the iron oxychalcogenides $La_2O_2Fe_2OM_2$ (M = S, Se). Elastic neutron scattering reveals that M = S and Se have similar nuclear structures at room and low temperatures. Our neutron diffraction data reveals that both materials obtain antiferromagnetic ordering at a Néel temperature T_N 90.1 ± 0.16 K and 107.2 ± 0.06 K for M = Se and S, respectively. The magnetic arrangements for both M = S, Se compounds are obtained through Rietveld refinement. We find the order parameter exponent β to be 0.129 ± 0.006 for M = Se and 0.133 ± 0.007 for M = S. Each of these values is near the Ising symmetry value of 1/8. This suggests that although lattice and electronic structural modifications result from chalcogen replacement, the nature of the magnetic interactions is similar in these materials.

DOI: 10.1103/PhysRevB.99.024109

I. INTRODUCTION

The discovery of superconductivity in iron pnictide (FePn) compounds has generated considerable interest because these materials seem to be the only current alternative to the cuprates for comparably high transition temperatures to the superconducting state. As with the cuprates, superconductivity in the FePn appears by doping electrons or holes into a magnetically ordered parent compound. An important question is whether the FePn parent compounds are on the verge of a metal-insulator transition [1,2]. In order to establish the so-called incipient Mott scenario [3] in FePn, it is important to identify the Mott insulating portion of the phase diagram of these materials. One way to drive an FePn into the Mott insulating phase is by reducing the electron kinetic energy t and increasing the electron correlation interaction U.

Specific attention has been given to iron oxychalcogenides [4–7] by investigators seeking to discover new iron-based materials in which high-T_c superconductivity might be obtained by doping the Mott insulating state [8–10]. The iron oxychalcogenides $La_2O_2Fe_2OM_2$ with M = (S, Se), denoted by $La_2O_2Fe_2O(S, Se)_2$ throughout the paper, provide a case study in this approach. These particular iron oxychalcogenides are parent compounds that have a composition such that the nominal valence of Fe is 2+ and contain an Fe square lattice, which is similar to, but expanded relative to the FePn. $La_2O_2Fe_2O(S, Se)_2$ were first reported to have insulating properties by Mayer *et al.* [11]. In addition, the crystal structure contains tetragonally ordered, FePn-like Fe planes for which chalcogens alternate above and below the iron atoms. Oxygen atoms are contained in the rare-earth layers remniscent of the charge resevoirs of high-T_c cuprates [8,11].

In addition, the electronic behavior of $La_2O_2Fe_2O(S, Se)_2$ has been investigated. Zhu *et al.*, using local density to dynamical mean-field theory (LDA + DMFT), predicted [8] Mott insulating behavior and band narrowing for both $La_2O_2Fe_2O(S, Se)_2$. Bulk transport and magnetic measurements, in addition to resonant inelastic x-ray scattering and soft x-ray absorption spectroscopy [12], provided experimental evidence that both systems are indeed Mott insulators [8]. Band narrowing within $La_2O_2Fe_2O(S, Se)_2$ has been proposed to lead to a Mott insulating state as well as enhanced electron correlation effects [8]. While exhibiting strongly correlated Mott insulating behavior, $La_2O_2Fe_2O(S, Se)_2$ compounds may offer tunability of their electronic properties near a metal-insulator transition. In Mott insulators, it has been observed that sizable electronic correlations drive new

*byron.freelon@louisville.edu

physical effects upon doping (electron or hole) and other external perturbations [13]. They can induce a range of interesting behavior including a pseudogap regime as in the case of $Na_2Fe_2OSe_2$ [6,14] or orbital-selective incoherent states that naturally yield coexistent insulating and bad metallic states as in cuprates or FePn [15–17]. Furthermore, iron oxychalcogenides can be tuned by transition-metal or chalcogen substitution [8], to produce novel electronic and magnetic phases at low temperature. The substitution of S and Se has been shown to alter the character of electronic partial density of states in this material class [8,12,18]. Even the presence of superconductivity in the iron oxychalcogenides has been of interest such that the effects of F-doping in $La_2O_{3-x}F_xFe_2Se_2$ and the substitution of Mn for Fe in $La_2O_2Fe_{1-x}Mn_xSe_2$ have been investigated; however, no superconductivity was observed [10,19,20].

In addition to interesting electronic properties, studies of the magnetic behavior of iron oxychalcogenides have been pursued. $A_2F_2TM_2OM_2$ where A = (Ba, Sr) have been the subject of recent studies [8,19–25] which showed that these materials order antiferromagnetically. Further, $Ba_2F_2Fe_2OSe_2$ was proposed to be an example of a compound with a frustrated antiferromagnetic (AFM) checkerboard spin lattice [22]. Other oxychalcogenides exhibit the onset of AFM ordering two-dimensional (2D) short-range magnetic correlation well above the Néel temperature T_N [26]. Stock and McCabe recently reviewed magnetic frustration and spin fluctuations in $La_2O_2Fe_2OSe_2$ [4] and other oxychalcogenides.

In this work, we study and compare the structural and magnetic properties of the iron oxychalcogenides $La_2O_2Fe_2OS_2$ and $La_2O_2Fe_2OSe_2$ using neutron powder diffraction (NPD). Our focus is on powder materials since single-crystalline samples remain difficult to produce. We measure the neutron diffraction intensity as a function of temperature and we examine the structural and magnetic distinctions between the two parent compounds at room and low temperatures. Section II provides the experimental details of the magnetic susceptibility and neutron diffraction measurements. Section III gives the results of nuclear and magnetic diffraction of both M = (S, Se) compounds. In addition, we discuss the magnetic structure and the magnetic order parameter behavior which reveal Ising symmetry in both materials. We provide a discussion of our findings within the context of specific magnetic exchange interactions and relative to other oxychalcogenide reports in the literature. Finally, our results are considered in light of some theoretical findings that have been reported on $La_2O_2Fe_2O(S, Se)_2$ systems.

II. EXPERIMENT

The samples studied here, $La_2O_2Fe_2O(S, Se)_2$, have nominal compositions and were prepared by a conventional solid-state reaction method using high-purity La_2O_3, S, Se, and Fe powders as starting materials. The powders were mixed in the stoichiometric ratios and carefully ground. Subsequently, the powders were pressed into pellets and then heated in an evacuated quartz tube at 1030 °C for 3 days; this process was repeated three times. The samples were confirmed to be of a single phase by the laboratory x-ray powder diffraction measurements [11].

NPD experiments were performed using the C2 high-resolution diffractometer at the NRU reactor at Chalk River Canadian Nuclear Labs. Room-temperature measurements were conducted with approximately 3 g of finely ground powder of both $La_2O_2Fe_2S_2$ and $La_2O_2Fe_2Se_2$. The samples were contained in vanadium cannisters sealed with indium gaskets under an atmosphere of He exchange gas. The low-temperature NPD measurements were conducted using the same cannisters. All handling of the powders was performed inside a He glovebox. The C2 diffractometer is equipped with an 800-wire position sensitive detector covering a range of 80°. Data were collected in the angular range from 5° to 117° 2θ using a Si (5 3 1) monochromator at wavelengths λ of 1.33 and 2.37 Å. Because λ is similar in scale as the atomic spacing, the incident neutrons can be Bragg diffracted by nuclear positions. Neutrons have zero charge and a fermionic

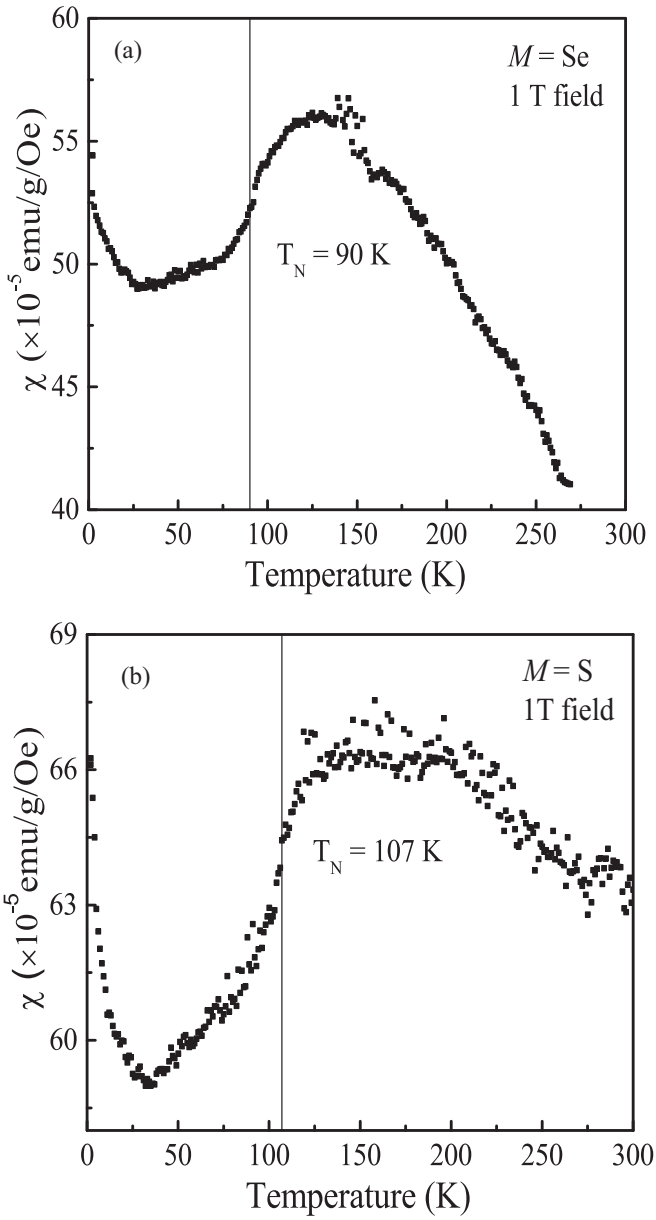

FIG. 1. The magnetic susceptibility of $La_2OFe_2O_2M_2$. (a) M = Se and (b) M = S.

$S = 1/2$; the resulting magnetic dipole moment of the neutron interacts with unpaired electrons to reveal magnetic ordering in solid materials. Rietveld analysis of the nuclear diffraction data estimated the samples to contain less than 1.2% and 1.3% of impurity phases in $La_2O_2Fe_2(S, Se)_2$, respectively.

Resistivity versus temperature data for $M =$ S and Se have been published in Refs. [8] and [12]. To examine the magnetic properties of these compounds, we measured magnetic susceptibility, $d\mathbf{M}/d\mathbf{H}$ as a function of temperature. The results are shown in Fig. 1; **M** is defined as the magnetization per unit volume and **H** is the applied magnetic field. The data were collected on powder samples with $H = 1$ T during warming using a magnetic properties measurement system manufactured by Quantum Design, Inc. The vertical lines in Fig. 1 serve as a guide to the eye and indicate the T_N whose determination is discussed below. The susceptibility data are similar to what is expected from 2D AFM samples except that there are Curie tails at low temperatures. This could indicate the presence of a small concentration of paramagnetic impurities. The Curie tails do not affect the susceptibility curves in the Néel regions.

III. RESULTS

A. Nuclear structure: $M =$ S, Se

Room-temperature data was collected for crystal structure refinement in order to avoid magnetic Bragg peak contributions in analyzing the structural details of these materials. Figures 2(a) and 2(b) show the results of Rietveld structural refinement of (a) $M =$ S and (b) $M =$ Se at 290 K for data collected with neutrons with a wavelength of λ of 1.33 Å. The crystal structure refinement of the powder neutron diffraction data was carried out using the FULLPROF [27] program suite, with the use of its internal tables for scattering lengths. Our data is consistent with previous reports on $M =$ Se [28]. Our results indicate that both $M =$ (S, Se) materials have similar nuclear structures with the space group $I4/mmm$ (No. 139) consistent with previous reports on $M =$ Se [11]. The quality of the presented fits can be assessed by the listed Rietveld fit criteria: R-pattern R_p, R-whole pattern R_{wp}, R-Bragg R_B and crystallographic factor R_f. For $M =$ Se, $R_p = 8.5\%$, $R_{wp} = 10.1\%$, $R_B = 2.5\%$, $R_f = 1.6\%$; $M =$ S, $R_p = 7.7\%$, $R_{wp} = 8.4\%$, $R_B = 1.9\%$, and $R_f = 1.2\%$. Figure 3(a) shows this crystal structure. A direct comparison of the Rietveld refinement parameters of $M =$ (S, Se) is given in Table I. Bond angles and atomic distances, extracted from Rietveld refinement parameters, are tabulated for comparison of $M =$ S and Se in Table I. For completeness Table III presents the atomic position of constituents of $La_2O_2Fe_2O(S, Se)_2$ with their respective Wyckoff symbols. We find that the Fe unit cell volume of $M =$ Se is larger than that of $M =$ S. This is reasonable given that the ionic radius of sulfur (100 pm) is smaller than selenium (115 pm), consistent with our finding that the lattice parameters of $La_2O_2Fe_2OS_2$ ($a = 4.0397$ Å, $c = 17.8782$ Å) are smaller than those of $La_2O_2Fe_2OSe_2$ ($a = 4.0849$ Å, $c = 18.5865$ Å). The interatomic distances we obtained are given in Table II. The Fe-Fe atomic distances $d_{\text{Fe-Fe}}$ are larger by 1.2% and 1.1%, as compared to LaFeOAs [29] for $M =$ Se and S, respectively. Rietveld analysis yielded measurements for the bond angles subtended by Se-Fe-Se and S-Fe-S defined as θ_1 and θ_2, respectively, as listed in Table II. These bonds define the distortion of the Fe(S, Se)$_4$ squares contained in the Fe_2OS_4 and Fe_2OSe_4 octahedra [cf. Fig. 3(a)], respectively.

$La_2O_2Fe_2O(S, Se)_2$ contain anti-CuO_2-type square, planar stacks such that $[La_2O_2]^{2+}$ layers and $[Fe_2O]^{2+}$ layers are separated by $(S, Se)^{2-}$ anions as seen in Fig. 3(a). The Fe^{2+} cations are linked through two in-plane oxygen O(2) anions as well as four out-of-plane (S^{2-}, Se^{2-}) anions. The Fe atoms are tetrahedrally coordinated with (S, Se) atoms alternatingly located above or below the center of the Fe-O plaquettes; therefore, the Fe-M layers are not flat. These D_{2h} point symmetry octahedra are face sharing such that the shared face is intersected by the Fe-Fe nearest-neighbor line of sight [21].

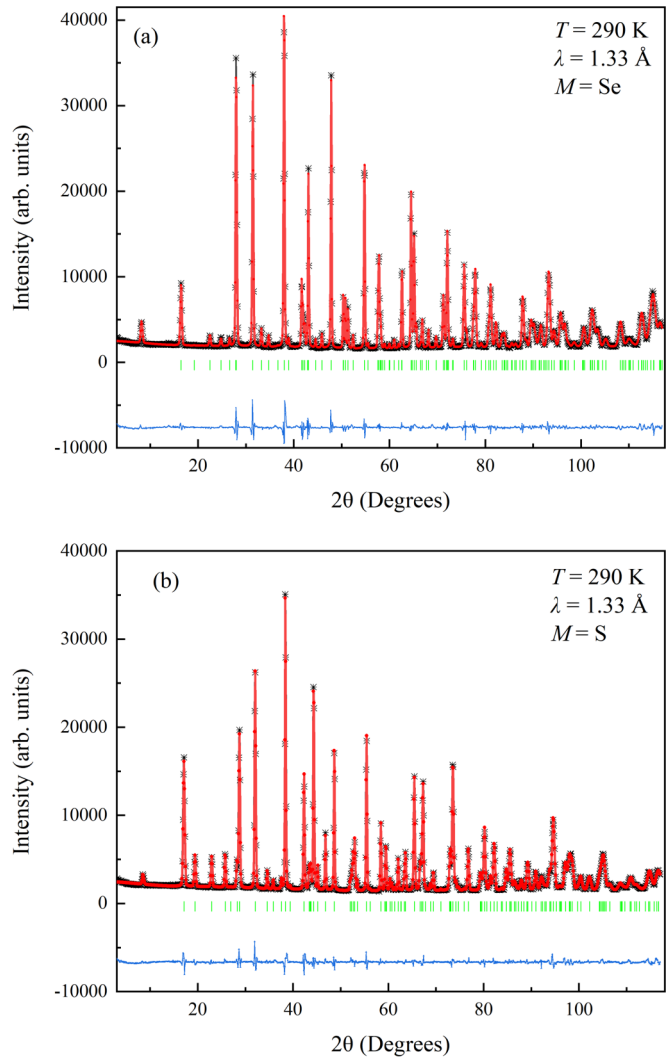

FIG. 2. Rietveld refinement profiles using (a) $M =$ Se and (b) $M =$ S at 290 K; data collected using the C2 diffractometer with wavelength λ = 1.33 Å. The data were refined using the space group $I4/mmm$. Observed and calculated patterns are shown in black and red, respectively, with the difference profile (blue) and nuclear Bragg peak positions shown as green vertical tick marks.

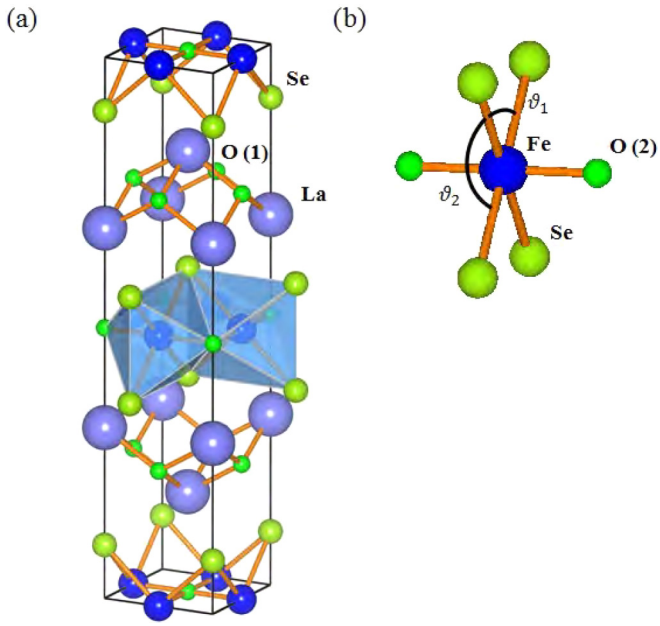

FIG. 3. The crystal structure of $La_2O_2Fe_2O(S, Se)_2$ is shown in (a). The coordination geometry of an Fe atom is shown in (b). The angles θ_1 and θ_2 are described in the text.

Here we list the angles θ_1 and θ_2 [see Fig. 3(b)] for M = S and Se along for a comparison with that of other oxychalcogenides. Specifically, $La_2O_2Fe_2OS_2$, 98.7° and 81.3°; $La_2O_2Fe_2OSe_2$, 97.2° and 82.8°; $Nd_2O_2Fe_2OSe_2$, 96.1° and 83.9° [30]; $La_2O_2Co_2OSe_2$, 98.7° and 81.3° [31]; $Sr_2Ti_2F_2OAs_2$, 96.3° and 83.7°; $Sr_2Ti_2F_2OSb_2$, 91.0° and 89.0° [32]; $Sr_2Fe_2F_2OS_2$, 100.2° and 79.8°; $Ba_2Fe_2F_2OS_2$, 102.2° and 77.8°; $Sr_2Fe_2F_2OSe_2$, 97.2° and 82.8° [22]. As seen this comparison of the θ_1 values for M = S, Se indicate that the S atoms are closer to the iron plane than Se chalcogens. This Fe-S distance results in greater octahedral distortion for the M = S material as compared to M = Se [33].

Our low-temperature, high-resolution, M = (S, Se) powder diffraction data does not contain pattern changes or structural Bragg peak splittings that would indicate the occurrence of a thermally driven structural phase transition. We do not observe the emergence of an atomic arrangement with lower symmetry as a function of temperature. This is consistent with the results for M = Se reported by Free and Evans [28]. Those authors noticed subtle temperature-dependent lattice behavior and atomic displacement parameter U_{33} trends in $La_2O_2Fe_2OSe_2$ [28]. It was suggested that these features were, at best, weak indications of a lowering of lattice symmetry. It has been proposed that the absence of a structural phase transition is due to the reduction of magnetostructural coupling in $La_2O_2Fe_2O(S, Se)_2$ caused by structural disordering [28].

TABLE I. Refined parameters for $La_2O_2Fe_2O(S, Se)_2$ at 290 K. B is the isotropic thermal parameter.

	$La_2OFe_2O_2Se_2$	$La_2OFe_2O_2S_2$
a (Å)	4.0849(6)	4.0397(0)
c (Å)	18.5865(0)	17.8782(0)
V (Å^3)	310.15(6)	291.76(0)
La B (Å^2)	0.33(5)	0.42(4)
Fe B (Å^2)	0.57(4)	0.52(4)
O(1) B (Å^2)	0.62(7)	0.58(5)
O(2) B (Å^2)	1.06(1)	1.14(9)
M B (Å^2)	0.54(6)	0.54(1)

A more detailed study of the local (short-range) structure of $La_2O_2Fe_2O(S, Se)_2$ was performed in order to determine whether there is any localized structural arrangement as a function of temperature; a pulsed neutron scattering study of the local structure of $La_2O_2Fe_2OSe_2$ was conducted from which atomic position deviations from radial distribution function data were extracted [34]. No local structure change from the low-temperature $I/4mmm$ symmetry was observed in these experiments consistent with our findings. Both Fuwa *et al.* [30] and Free and Evans [28] suggested that the absence of structural phase transitions might be due to the lack of magnetostriction or magnetoelastic coupling in $La_2O_2Fe_2OSe_2$ [6,35].

B. Magnetic structure: M = S, Se

Upon cooling, we observe extraneous intensity in the diffraction profiles of M = S and Se which we attributed to magnetic phase transition behavior. These peaks were assigned a magnetic origin on the basis of their temperature dependence and the complete Rietveld refinement of the diffraction patterns. The Se end member has been well characterized by Free and Evans [28]. It was argued [28] that the AFM3 model [36] provides the best fit to the magnetic structure of the Se end member. We used the SARAH suite of programs [37] to analyze the representations and provide the basis vectors for refinement with FULLPROF [27,38]. The AFM3 model

TABLE II. Interatomic distances and angles of $La_2O_2Fe_2O(S, Se)_2$ at 290 K.

$La_2O_2Fe_2OSe_2$				$La_2O_2Fe_2OS_2$			
Length	(Å)	Bond angle	(deg)	Length	(Å)	Bond angle	(deg)
$d_{Fe\text{-}Fe}$	2.89050(3)	Fe-O-Fe (2)	90.00	$d_{Fe\text{-}Fe}$	2.85813(0)	Fe-O-Fe (2)	90.00
$d_{Fe\text{-}O2}$	2.04389(3)	Fe-Se-Fe	64.086	$d_{Fe\text{-}O2}$	2.02100(0)	Fe-S-Fe	64.919
$d_{Fe\text{-}Se}$	2.72400(4)	Se-Fe-Se	97.237	$d_{Fe\text{-}S}$	2.66264(0)	S-Fe-S	98.755
$d_{La\text{-}O1}$	2.38013(3)	La-O-La (1)	118.348	$d_{La\text{-}O1}$	2.33787(0)	La-O-La (1)	119.642
$d_{La\text{-}Se}$	3.31832(4)			$d_{La\text{-}S}$	3.26261(0)		

TABLE III. Atomic positions of $La_2O_2Fe_2O(S, Se)_2$ at 290 K extracted from refined parameters.

$La_2O_2Fe_2OSe_2$					$La_2O_2Fe_2OS_2$				
Atom	Site	x	y	z	Atom	Site	x	y	z
La	4*e*	0.5000	0.5000	0.1842	La	4*e*	0.5000	0.5000	0.18084
Fe	4*c*	0.5000	0.0000	0.0000	Fe	4*c*	0.5000	0.0000	0.0000
Se	4*e*	0.0000	0.0000	0.0963	S	4*c*	0.0000	0.0000	0.0934
O1	4*d*	0.5000	0.0000	0.2500	O1	4*d*	0.5000	0.0000	0.2500
O2	2*b*	0.5000	0.5000	0.0000	O2	2*b*	0.5000	0.5000	0.0000

may be written as $\mathrm{Fe}\{1/2, 0, 0\}\Gamma_2\psi_1 + \mathrm{Fe}\{1/2, 0, 0\}\Gamma_3\psi_2$, the irreducible representations being labeled with the scheme of Kovalev [39] and the basis vectors that of Sarah [37]. $\Gamma_2\psi_1$ and $\Gamma_3\psi_2$ generate the same geometric ordering scheme on the two independent sites; during refinement, the standard Fe^{2+} magnetic form factor is assumed, and the additional constraint is applied that both independent sites possess the same size ordered magnetic moment.

We initially verified the AFM3 model [36] also gives the best fit to the magnetic structure of our data from the $La_2O_2Fe_2OSe_2$ compound. In close similarity to what was described previously for $M =$ Se, our analysis of the magnetic structure of the $M =$ S compound reveals that the magnetic cell of $M =$ S is commensurate and is doubled in a and c with respect to the structural cell. The magnetic ordering in $La_2O_2Fe_2OS_2$ is associated with an ordering vector $\mathbf{k} = (1/2, 0, 1/2)$, and the single Fe site on $\{1/2, 0, 0\}$ in the nuclear $I4/mmm$ cell is described by two distinct orbits governing the two $\{1/2, 0, 0\}$ and $\{0, 1/2, 0\}$ Fe sites that are independent in the magnetically ordered state. In Fig. 4 the low angle region of the powder diffractograms of $La_2O_2Fe_2OS_2$ is shown at 290 K [panel (a)] and 4 K [panel (b)]. The data (Observed) are presented in order to show magnetic Bragg peaks $\mathbf{Q}_M = (000), (-101), (002)$, and (-103) (blue label) that develop at low temperatures in addition to the structural Bragg peaks are present (red) for both high and low temperatures. In addition to the data, the Rietveld refinement fits (Calculated) are shown in both temperature regions.

There are two independent Fe sites for both $La_2O_2Fe_2O(S, Se)_2$. By performing a full Rietveld refinement and analysis of the neutron powder diffraction data, the ordered Fe^{2+} moment of $La_2O_2Fe_2OS_2$ was determined to be $2.32(4)\mu_B$ at 4 K. For $La_2O_2Fe_2OSe_2$ a range of values from 2.8 to $3.50(5)\mu_B$ has been reported [40]. Thus the magnetic ground state of both compounds is composed of the Fe ions in a high spin, noncollinear antiferromagnetically ordered state.

In order to discuss the magnetic structure results obtained for $La_2O_2Fe_2O(S, Se)_2$ from our analysis, we summarize the most prominent description of the spin interactions considered for these materials. Several spin interaction labeling conventions can be found in the literature on $La_2O_2Fe_2OSe_2$; Table IV lists them. We adopt the convention used in Refs. [8,28,40]. The spin Hamiltonian for $La_2O_2Fe_2O(S, Se)_2$ has been modeled by Zhu *et al.* [8] using three interactions J_1, J_2, and J_2'. J_1 has several contributions: (a) a face-sharing 64° interaction between Fe-Se-Fe, (b) an Fe-O-Fe 90° interaction, and (c) possibly an iron nearest-neighbor (NN) contribution. J_2 is a next-nearest-neighbor (NNN) interaction that consists of a 98° edge-sharing term involving Fe-Se-Fe contributions from two buckled Se atoms. J_2' is a NN, 180° Fe-O-Fe interaction between the corner-sharing octahedra. Figure 5 provides a schematic description of these interactions.

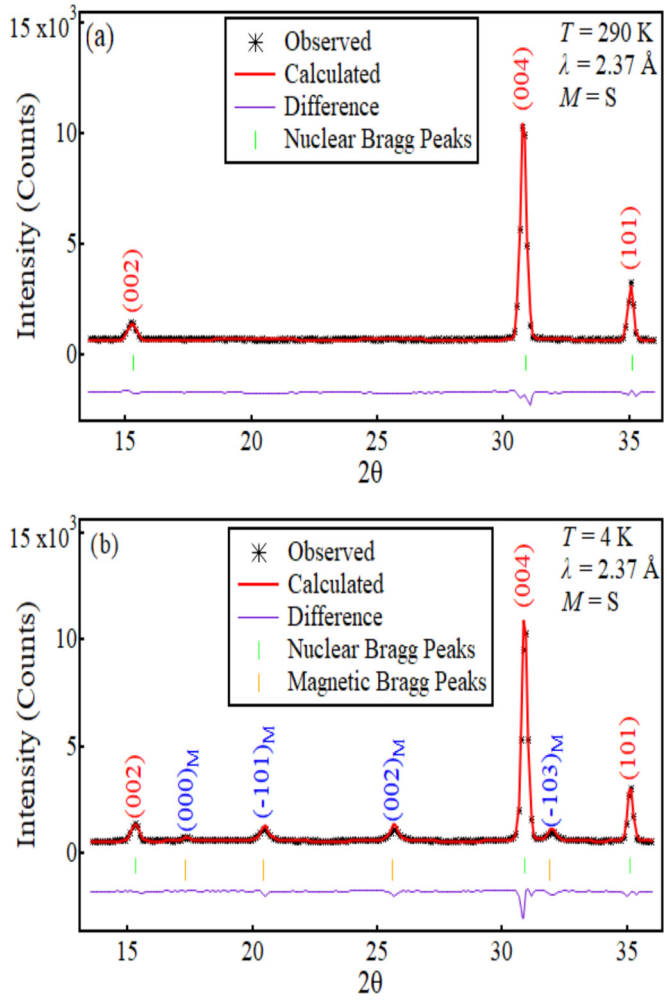

FIG. 4. Refined fits (Calculated) of neutron powder diffraction data (Observed) at low angle for $La_2O_2Fe_2OS_2$ is shown for (a) 290 K and (b) 4 K. Red (blue) labels indicate the (HKL) indices of the nuclear (magnetic) Bragg diffraction peaks. The difference (purple) is Observed − Calculated.

TABLE IV. Magnetic interaction naming conventions. Note: The (next-) nearest-neighbor interactions are (N) NN.

Interaction	Description	Geometry	Refs. [8,28,40][a]	Refs. [19,22,33]
NNN	Fe-O-Fe	180°	J_2'	J_1
NN	TM-TM	In-plane	J_1	J_3
NNN	TM-*M*-TM	∼90°	J_2	J_2

[a]This work.

Using the interaction (J_1, J_2, J_2') labeling, Zhu *et al.* employed a generalized gradient approximation + Coulomb energy U calculation [8] and determined that the magnetic ground state of $La_2O_2Fe_2OSe_2$ should obtain either the AFM1 or the AFM6 (cf. Fig. 6 in Ref. [28]) configuration depending on the value of U. By contrast, Free and Evans [28] reported that elastic neutron-scattering results indicated that the magnetic moments of $La_2O_2Fe_2OSe_2$ should order in the AFM3 [see Fig. 6(a)] frustrated, collinear configuration similar to $Fe_{1.086}Te$. At variance with this finding, McCabe *et al.* concluded that inelastic neutron scattering (INS) results on $La_2O_2Fe_2OSe_2$ are consistent with a multicomponent, noncollinear 2-*k* magnetic structure shown in Fig. 6(b). The 2-*k* structure is made up of two orthogonal stripes within the Fe_2OM_2 layers. While the AFM3 configuration provided good fits to our M = S and Se neutron diffraction data, as noted by Ref. [40], neutron powder diffraction cannot distinguish between the various AFM models that have been proposed for $La_2O_2Fe_2OSe_2$. Therefore the consistency between INS data and the 2-*k* magnetic structure offer insight to understanding the magnetic structures of $La_2O_2Fe_2O(S, Se)_2$ given that the production of single crystals is difficult. In addition to neutron scattering experiments, nuclear magnetic resonance (NMR) measurements by Gunther *et al.* [41] and Ref. [42] were interpreted to suggest that the 2-*k* model is the appropriate description of the M = Se.

Magnetic frustration has been addressed in $La_2O_2Fe_2OSe_2$ and other iron oxychalcogenides. Some amount of frustration in $La_2O_2Fe_2O(S, Se)_2$ is to be expected given that there are FM (J_2) and AFM (J_2') interactions associated with the FeOM_2 layer. These competing interactions, in addition to magnetocrystalline anisotropy, create a frustrated spin environment in which the FeOM_2 layer has three principal competing magnetic interactions J_1, J_2, and J_2' [33]. In contrast to the AFM3 collinear frustrated model of Ref. [28], McCabe *et al.* suggested the 2-*k* $La_2O_2Fe_2OSe_2$ structure to be weakly frustrated due to the magnetic configuration being collectively stabilized by the AFM J_2' and FM J_2 interactions as well as the magnetocrystalline anisotropy. Those authors reported that both the magnetic frustration and the exchange coupling are weak in $La_2O_2Fe_2OSe_2$ compared to other iron oxychalcogenides. The variance in these reports suggests that the extent of magnetic frustration in $La_2O_2Fe_2OS_2$ and $La_2O_2Fe_2OSe_2$ is not fully understood; however, it is still possible to compare the magnetic frustration of M = S and Se. As seen above, our structural refinements yield a smaller bond angle Fe-*M*-Fe in M = S than for M = Se. This is an indication that the M = S NNN distances are smaller and, therefore, have increased magnetic exchange interaction. In addition, the NN exchange of M = S is increased relative to that of M = Se. It has been proposed [30] that the NNN AFM interaction J_2' in iron oxychalcogenides such as $Nd_2O_2Fe_2OSe_2$ is due to the Goodenough-Kanamori rule [43]. This reasoning might explain the difference in Néel temperatures observed for M = S and M = Se.

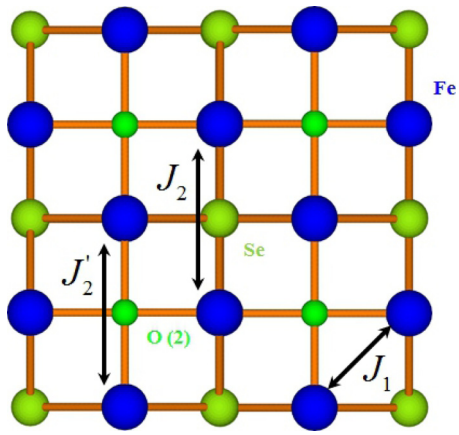

FIG. 5. Spin interactions J_1, J_2, and J_2' used in modeling the magnetic behavior of $La_2O_2Fe_2O(S, Se)_2$. These are the principle spin interactions contained in the $Fe_2O(S, Se)_2$ layer. The details regarding each exchange constant are given within the text.

Several spin Hamiltonians have been introduced in order to address the magnetic behavior of materials thought to be within strong-coupling limit, e.g., iron oxychalcogenides and iron alkaline selenides $A_{0.8}Fe_{1.6}Se_2 \rightarrow A_2Fe_4Se_5$ (referred to as "245s" where A = Rb, Cs, K, and Tl) [44–47]. Unlike the FePn, the increased electron correlation of the iron chalcogenides and iron alkaline selenides leads to narrower iron bandwidths. Consequently, despite the absolute value of the Hunds coupling being similar to that of the pnictides ($J_H \sim 0.7$ eV), its role is more pronounced, resulting in a larger spin $S = 2$. Importantly, INS experiments [40] have yielded $S = 2$ for $La_2O_2Fe_2OSe_2$ and $Rb_{0.8}Fe_{1.5}S_2$ [48].

Finally, the absence of $La_2O_2Fe_2O(S, Se)_2$ structural phase transitions can be compared to the FePn compounds, which actually undergo a structural phase transition from tetragonal to orthorhombic symmetry at a structural transition temperature T_S. In the case of FePn, a structural phase transition is either concomitant with or immediately prior to an AFM phase transition. The presence of ferro-orbital ordering of the $d_{xz,yz}$ states is intimately linked to the FePn structural phase transitions. Furthermore, FePn ferro-orbital ordering is associated with magnetic phase changes by virtue of spin-orbit coupling and Coulomb interaction [35]. By contrast, the absence of ferro-orbital ordering in $La_2O_2Fe_2O(S, Se)_2$ may be due to the apparent nondegeneracy of the $d_{xz,yz}$ orbitals [12].

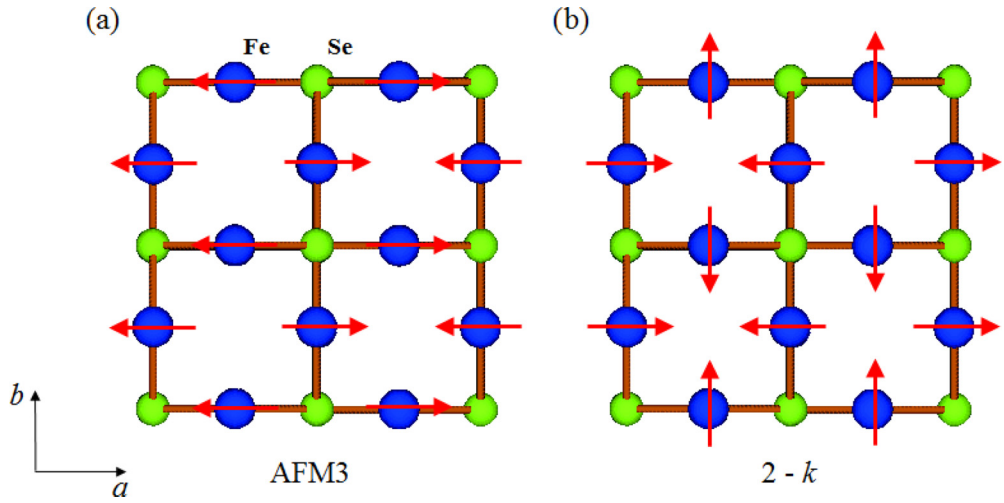

FIG. 6. The (a) collinear AFM3 and (b) noncollinear 2-k magnetic structure models for $La_2O_2Fe_2OSe_2$.

C. Magnetic order parameter critical behavior

To determine the thermal dependence of the magnetic ordering behavior of $M = (S, Se)$, the intensity of the magnetic Bragg peak $\mathbf{Q_m} = (-103)$ was measured over a temperature range of 300 K to 4 K in each material. The results for both $La_2O_2Fe_2O(S, Se)_2$ compounds are plotted in Fig. 7. The peak intensity can be used as a measure of the magnetic order parameter squared, ϕ^2. $La_2O_2Fe_2O(S, Se)_2$ peak intensity data was fitted to the power-law functional form $\phi^2(T/T_N) = (1 - T/T_N)^{2\beta_{Fe}}$ [49]. β_{Fe}, the critical exponent, and T_N, the Néel temperature, served as adjustable fit parameters. Fits were applied over the temperature range $0.05 \leqslant T/T_N \leqslant 1$ and yielded values for β_{Fe} and T_N of 0.129 ± 0.006 and 90.10 ± 0.16 K for $M =$ Se and 0.133 ± 0.007 and 107.20 ± 0.06 K in the case of $M =$ S. The Néel transition temperatures from this analysis are consistent with those obtained from magnetic susceptibility measurements we discussed earlier. In addition, the exponents β_{Fe} extracted here are close to those reported for $M =$ Se in Ref. [28]. Furthermore, the β_{Fe} for both $M =$ S and Se are close to the Ising critical exponent β_{Ising} value of 1/8. This result indicates that the magnetic phase transitions in $La_2O_2Fe_2OS_2$ and $La_2O_2Fe_2OSe_2$ may be weakly first order in agreement with results obtained using Mössbauer spectroscopy [42].

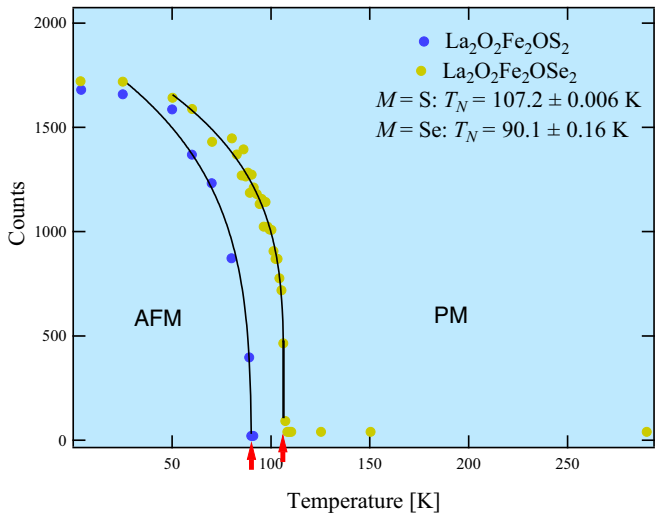

FIG. 7. The magnetic order parameter is shown at the (1, 0, 3) magnetic Bragg reflection. The peak intensity measured at $\mathbf{Q} = (1, 0, 3)$, plotted for both $La_2O_2Fe_2O(S, Se)_2$, is used as a measure of the magnetic order parameter ϕ^2.

These critical exponent values also suggest that there are 2D Ising-like spin fluctuations near the critical point. The similarity of the critical exponents is further indication that the magnetic phases of $La_2O_2Fe_2OS_2$ and $La_2O_2Fe_2OSe_2$ arise from similar magnetic interaction geometries.

IV. CONCLUSIONS

We have presented a comparison of the structural and magnetic properties of the homologs $La_2O_2Fe_2O(S, Se)_2$ based on susceptibility and neutron powder diffraction data. Our motivation was to present a comparison of the structural and magnetic details of $M =$ S and Se as there had been no previously published, explicit comparison of these compounds. Neutron powder diffraction indicates that the nuclear structures of $La_2O_2Fe_2O(S, Se)_2$ are similar to the structural character found in other oxychalcogenides with the main distinction being the difference in lattice size based on the atomic radii of the two chalcogens. Nuclear Bragg diffraction data indicates that the FeO_2Se_4 and FeO_2S_4 octahedra have different sizes; this produces different magnitudes of distortion within the octahedra. This distortion is expected to be related to the presence of the relatively high extent of electron correlation compared to the FePn. In addition, the distorted octahedra can diminish magnetoelastic coupling by precluding orbital ordering that is necessary to establish a link between the magnetic phase transition and a structural phase transformation [33]. We did not observe structural phase transitions in either of these materials. Nor did we see evidence of a nematic phase similar to that which exists in the FePn compounds. However, observing only a magnetic phase transition from the high-temperature paramagnetic phase to a lower temperature AF phase, we used group theory and magnetic refinement methods to determine the

magnetic structure of these materials. The magnetic structure of $La_2O_2Fe_2O(S, Se)_2$ was determined to be consistent with a noncollinear 2-k configuration up to the basic limitations imposed by the use of powder samples. 2D Ising symmetry was determined for both $La_2O_2Fe_2O(S, Se)_2$. We discussed models of frustrated magnetism and their relevance to metallic and insulating behavior iron oxychalcogenides.

ACKNOWLEDGMENTS

We are grateful to the technical staff at CNBC for excellent support. Work at Lawrence Berkeley National Laboratory and UC Berkeley was supported by the Office of Science, Office of Basic Energy Sciences (BES), Materials Sciences and Engineering Division of the U.S. Department of Energy (DOE) under Contract No. DE-AC02-05-CH1231 within the Quantum Materials Program (KC2202) and BES. The work at Zhejiang University was supported by the National Basic Research Program of China (973 Program) under Grants No. 2011CBA00103 and No. 2012CB821404, the National Science Foundation of China (Grants No. 11374261 and No. 11204059), and Zhejiang Provincial Natural Science Foundation of China (Grant No. LQ12A04007). M.S.L. thanks MPIPKS, Dresden for hospitality. L.C.'s work was supported by CNPq (Grant No. 307487/2014-8). L.C. also thanks the Physical Chemistry Department at Technical University Dresden for hospitality.

[1] E. Abrahams and Q. Si, J. Phys.: Condens. Matter **23**, 223201 (2011).
[2] R. Yu, Q. Si, P. Goswami, and E. Abrahams, J. Phys.: Conf. Ser. **449**, 012025 (2013).
[3] J. Dai, Q. Si, J.-X. Zhu, and E. Abrahams, Proc. Natl. Acad. Sci. USA **106**, 4118 (2009).
[4] C. Stock and E. E. McCabe, J. Phys.: Condens. Matter **28**, 453001 (2016).
[5] G. Jin, Y. Wang, X. Dai, X. Ren, and L. He, Phys. Rev. B **94**, 075150 (2016).
[6] L. Craco, M. S. Laad, and S. Leoni, J. Phys.: Condens. Matter **26**, 145602 (2014).
[7] R. K. Oogarah, C. P. J. Stockdale, C. Stock, J. S. O. Evans, A. S. Wills, J. W. Taylor, and E. E. McCabe, Phys. Rev. B **95**, 174441 (2017).
[8] J.-X. Zhu, R. Yu, H. Wang, L. L. Zhao, M. D. Jones, J. Dai, E. Abrahams, E. Morosan, M. Fang, and Q. Si, Phys. Rev. Lett. **104**, 216405 (2010).
[9] H. Lei, H. Ryu, V. Ivanovski, J. B. Warren, A. I. Frenkel, B. Cekic, W.-G. Yin, and C. Petrovic, Phys. Rev. B **86**, 195133 (2012).
[10] S. Landsgesell, K. Prokeš, C. Colin, D. Abou-Ras, and N. Schäfer, J. Supercond. Novel Mag. **28**, 1111 (2015).
[11] J. M. Mayer, L. F. Schneemeyer, T. Siegrist, J. V. Waszczak, and B. Van Dover, Angew. Chem., Int. Ed. Engl. **31**, 1645 (1992).
[12] B. Freelon, Y. H. Liu, J.-L. Chen, L. Craco, M. S. Laad, S. Leoni, J. Chen, L. Tao, H. Wang, R. Flauca, Z. Yamani, M. Fang, C. Chang, J.-H. Guo, and Z. Hussain, Phys. Rev. B **92**, 155139 (2015).
[13] Y. T. M. Imada, A. Fujimori, Rev. Mod. Phys. **70**, 1039 (1998).
[14] T.-P. Choy and P. Phillips, Phys. Rev. Lett. **95**, 196405 (2005).
[15] G. S. Boebinger, Y. Ando, A. Passner, T. Kimura, M. Okuya, J. Shimoyama, K. Kishio, K. Tamasaku, N. Ichikawa, and S. Uchida, Phys. Rev. Lett. **77**, 5417 (1996).
[16] K. Semba and A. Matsuda, Phys. Rev. Lett. **86**, 496 (2001).
[17] J. W. Simonson, K. Post, C. Marques, G. Smith, O. Khatib, D. N. Basov, and M. C. Aronson, Phys. Rev. B **84**, 165129 (2011).
[18] H. Zhang, X. Wu, D. Li, S. Jin, X. Chen, T. Zhang, Z. Lin, S. Shen, D. Yuan, and X. Chen, J. Phys.: Condens. Matter **28**, 145701 (2016).
[19] H. Lei, E. S. Bozin, A. Llobet, V. Ivanovski, V. Koteski, J. Belosevic-Cavor, B. Cekic, and C. Petrovic, Phys. Rev. B **86**, 125122 (2012).
[20] S. Landsgesell, K. Prokeš, T. Hansen, and M. Frontzek, Acta Mater. **66**, 232 (2014).
[21] D. G. Free, N. D. Withers, P. J. Hickey, and J. S. O. Evans, Chem. Mater. **23**, 1625 (2011).
[22] H. Kabbour, E. Janod, B. Corraze, M. Danot, C. Lee, M.-H. Whangbo, and L. Cario, J. Am. Chem. Soc. **130**, 8261 (2008).
[23] Y. Fuwa, T. Endo, M. Wakeshima, Y. Hinatsu, and K. Ohoyama, J. Am. Chem. Soc. **132**, 18020 (2010).
[24] S. Landsgesell, E. Blumenröther, and K. Prokeš, J. Phys.: Condens. Matter **25**, 086004 (2013).
[25] Y. Liu, S. Zhang, W. Lu, L. Li, S. Tan, B. Yuan, J. Chen, and Y. Sun, J. Alloys Compd. **618**, 263 (2015).
[26] J. B. He, D. M. Wang, H. L. Shi, H. X. Yang, J. Q. Li, and G. F. Chen, Phys. Rev. B **84**, 205212 (2011).
[27] J. Rodriguez-Carvajal, Physica B (Amsterdam) **192**, 55 (1993).
[28] D. G. Free and J. S. O. Evans, Phys. Rev. B **81**, 214433 (2010).
[29] K. Haule, J. H. Shim, and G. Kotliar, Phys. Rev. Lett. **100**, 226402 (2008).
[30] Y. Fuwa, M. Wakeshima, and Y. Hinatsu, J. Phys.: Condens. Matter **22**, 346003 (2010).
[31] Y. Fuwa, M. Wakeshima, and Y. Hinatsu, Solid State Commun. **150**, 1698 (2010).
[32] D. Charkin, V. Plotnikov, A. Sadakov, O. Omel'yanovskii, and S. Kazakov, J. Alloys Compd. **509**, 7344 (2011).
[33] Y. Liu, S. Zhang, S. Tan, B. Yuan, X. Kan, L. Zu, and Y. Sun, J. Solid State Chem. **221**, 272 (2015).
[34] K. Horigane, K. Kawashima, S. Ji, M. Yoshikawa, D. Louca, and J. Akimitsu, Proceedings of the International Conference on Strongly Correlated Electron Systems (SCES 2013) [JPS Conf. Proc. **3**, 015039 (2014)].
[35] W. Lv, J. Wu, and P. Phillips, Phys. Rev. B **80**, 224506 (2009).
[36] C. Fang, B. A. Bernevig, and J. Hu, Europhys. Lett. **86**, 67005 (2009).
[37] A. Wills, Physica B (Amsterdam) **276**, 680 (2000).
[38] T. Roisnel and J. Rodríguez-Carvajal, European Powder Diffraction EPDIC 7, Mater. Sci. Forum **378**, 118 (2001).
[39] O. V. Kovalev, *Representations of the Crystallographic Space Groups* (Gordon and Breach Science, Switzerland, 1993).

[40] E. E. McCabe, C. Stock, E. E. Rodriguez, A. S. Wills, J. W. Taylor, and J. S. O. Evans, Phys. Rev. B **89**, 100402 (2014).

[41] M. Günther, S. Kamusella, R. Sarkar, T. Goltz, H. Luetkens, G. Pascua, S.-H. Do, K.-Y. Choi, H. D. Zhou, C. G. F. Blum, S. Wurmehl, B. Büchner, and H.-H. Klauss, Phys. Rev. B **90**, 184408 (2014).

[42] B. Freelon, R. Sarkar, S. Kamusella, F. Brückner, V. Grinenko, S. Acharya, M. Laad, L. Craco, Z. Yamani, R. Flacau, I. Swainson, Y. Liu, H. Wang, J. Du, M. Fang, and H.-H. Klauss, arXiv:1708.01693.

[43] J. Kanamori, Prog. Theor. Biol. **17**, 177 (1957).

[44] Q. Si, R. Yu, and E. Abrahams, Nat. Rev. Mater. **1**, 16017 (2016).

[45] P. Bilbao Ergueta and A. H. Nevidomskyy, Phys. Rev. B **92**, 165102 (2015).

[46] S.-S. Gong, W. Zhu, D. N. Sheng, and K. Yang, Phys. Rev. B **95**, 205132 (2017).

[47] R. Yu and A. H. Nevidomskyy, J. Phys.: Condens. Matter **28**, 495702 (2016).

[48] M. Wang, P. Valdivia, M. Yi, J. X. Chen, W. L. Zhang, R. A. Ewings, T. G. Perring, Y. Zhao, L. W. Harriger, J. W. Lynn, E. Bourret-Courchesne, P. Dai, D. H. Lee, D. X. Yao, and R. J. Birgeneau, Phys. Rev. B **92**, 079901 (2015).

[49] S. D. Wilson, Z. Yamani, C. R. Rotundu, B. Freelon, E. Bourret-Courchesne, and R. J. Birgeneau, Phys. Rev. B **79**, 184519 (2009).